Indigo: A Natural Molecular Passivator for Efficient Perovskite Solar Cells

Junjun Guo, Jianguo Sun, Shiwen Fang, Xufeng Ling, Xuliang Zhang, Yao Wang, Hehe Huang, Chenxu Han, Long Hu, Zizhen Zhou, Claudio Cazorla, Dewei Chu, Tom Wu, Jianyu Yuan, Wanli Ma**

J. Guo, J. Sun, S. Fang, X. Ling, Y. Wang, H. Huang, C. Han, Prof. J. Yuan, Prof. W. Ma
Institute of Functional Nano & Soft Materials (FUNSOM), Jiangsu Key Laboratory for Carbon-Based Functional Materials & Devices, Soochow University, 199 Ren-Ai Road, Suzhou Industrial Park, Suzhou, Jiangsu 215123, P. R. China.
E-mail: jyyuan@suda.edu.cn (J. Y.), wlma@suda.edu.cn (W. M.)

L. Hu
School of Engineering, Macquarie University, Sydney, New South Wales 2109, Australia.

Z. Zhou, Prof. D. Chu, Prof. T. Wu
School of Materials Science and Engineering, University of New South Wales (UNSW), Sydney, NSW 2052, Australia.

Prof. C. Cazorla
Departament de Física, Universitat Politècnica de Catalunya, Campus Nord B4-B5, E-08034 Barcelona, Spain

Keywords: Indigo, perovskite solar cells, passivation, natural dye, long-term stability.

Abstract: Organic-inorganic hybrid lead halide perovskite solar cells have made unprecedented progress in improving photovoltaic efficiency in the past decade, while still facing critical stability challenges. Herein, a naturel organic dye Indigo was first explored to be an efficient molecular passivator to assist the preparation of high-quality hybrid perovskite film with reduced defects and enhanced stability. The Indigo molecule with both carbonyl and amino groups can provide bifunctional chemical passivation for shallow-level defects. In-depth theoretical and experimental studies show that the Indigo can bind firmly with perovskite, enhancing the crystallization process of perovskite film with better morphology. Consequently, the Indigo-passivated perovskite film exhibits increased grain size with better uniformity, reduced grain boundaries and lower defect density, boosting the device efficiency up to ~23.0%. Furthermore, the Indigo passivation can enhance device stability both in terms of humidity and thermal stress. We believe these results not only gain insights into the multi-passivation role of

natural organic dye, but also provide simple yet efficient strategy using Indigo derivatives to prepare high quality hybrid perovskite film for optoelectronic application.

1. Introduction

The organic-inorganic lead halide perovskites have emerged and quickly become the most promising materials for solution-processed solar cells.[1-2] These hybrid semiconductors exhibit unique properties like high carrier mobility, long carrier diffusion length, high defect tolerance, low exciton binding energy.[3-5] Benefiting from these unique properties, the power conversion efficiency (PCE) of perovskite solar cells (PSCs) has rapidly increased from initial ~3% to now 25.5%,[6-8] situating it at the forefront of the third-generation solar cells.[9-10] In these polycrystalline hybrid perovskite film, defects formed at either surface or grain boundaries have been widely reported to significantly restrict carriers transport and crystal stability, which further deteriorates the device performance.[11-12] During the past decade, lots of passivation methods have been developed to enhance both efficiency and long-term stability of hybrid PSCs.[13-15]

These ionic hybrid perovskite materials are extremely sensitive to light[16-17], heat[18], and moisture[19], resulting in unstable crystal structure. Indeed, a great number of defects are generated during the film crystallization process due to the low formation energy and soft lattice character of the perovskite crystals.[20-21] Besides, the ionic nature of hybrid halide perovskite leads to unfavorable carrier recombination and ion migration within the perovskite film, resulting in unsatisfactory efficiency and stability of the device.[22-23] In specific, these defects formed during crystallization process mainly including defects at grain boundaries and surface, metallic lead clusters, and intrinsic point defects.[23-25] Among them, intrinsic site defects include uncoordinated Pb^{2+}/I^{-}, Pb-I antisites/impurities and surface defects due to terminally growth of perovskite crystals, significantly hindering the optoelectronic properties of the PSCs.[26-27] In order to eliminate these undesired defects, strategies such as component

engineering,[28-29] dimensionality engineering,[30-31] grain boundary engineering,[24] additive engineering,[32] and anti-solvent/solution engineering[33] have been intensively explored and investigated. Among these strategies, anti-solution treatment using functional passivating agents like organic molecules,[22] polymers[34], and inorganic nanocrystals[35] have been reported to effectively optimize the crystallization process as well as passivate the defects at surface and grain boundaries. For instance, Lewis bases containing isolated electron pairs in molecules framework, like carbonyl (C=O),[25] sulfoxide (S=O),[36] phosphate (P=O),[12] and cyano (-CN),[37] while positively charged intrinsic site defects on the surface of perovskite are called Lewis acids.[27] Yang *et al.* demonstrated that the amino group (-NH) in theophylline can interact with the I^- in the PbI_6^{2-} octahedron *via* hydrogen bonding and assist the carbonyl group (C=O) to interact with the uncoordinated Pb^{2+}.[15] Quite recently, Gao *et al.* reported the passivating the Pb-I antisites by the -NH and the metal Pb cluster by -OH of the protonic group using tailored molecule 4OH-NMI. In general, these highly effective passivator molecules contains intrinsically stable chemical structures as well as possessing isolated electron pairs unique to Lewis base groups.[38]

Inspired by our previous study in Isoindigo-based conjugated materials,[39] here, we first report a natural small organic dye Indigo as an efficient molecular passivator for efficient PSCs. Indigo molecule bears target carbonyl and amino functional groups; besides, it is very cheap, available from nature, and stable under heat, and moisture stresses, which is ideal for developing high performance PSCs. The carbonyl group (electron pair donor) in the Lewis Indigo molecule can interact with the unfilled *p*-orbitals Lewis acid Pb^{2+}, Pb-I antisites defect on the surface of the perovskite, and the amino group can interact with the I^-. In addition, the hydrogen bonding between Indigo and perovskite can restrain ion migration,[15] thus enhancing the stability of perovskite crystal structure. Correspondingly, the PCE of the Indigo passivated PSCs is enhanced from 20.18% to 22.91% with simultaneously increased short-circuit current (J_{sc}), open-circuit voltage (V_{oc}) and fill factor (*FF*) as well as reduced hysteresis relative to the

control one. Furthermore, due to the more hydrophobic surface and hydrogen bonding with the perovskite after Indigo passivation, the stability of the PSCs under humidity and thermal stress is enhanced.

2. Results and discussion

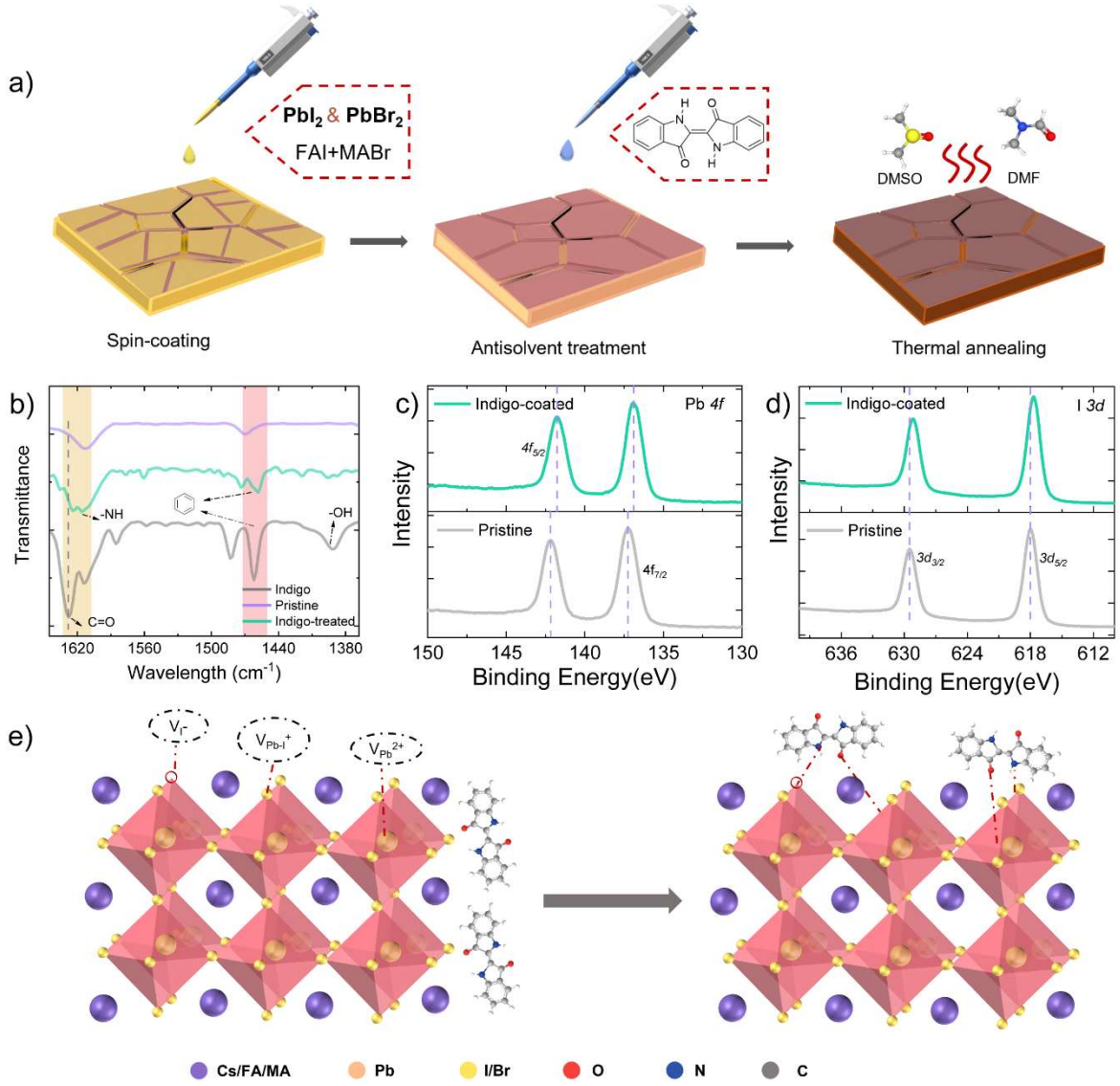

Figure 1. a) Schematic illustration of spin-coating process for fabricating perovskite films with Indigo-assisted antisolvent process, b) FTIR spectra of neat Indigo, pristine and Indigo passivated perovskites, c) Pb *4f* and d) I *3d* XPS spectra of pristine and passivated perovskite films, e) Schematic illustration of the passivating mechanism between Indigo and mixed hybrid perovskite.

As shown in **Figure 1a**, the 3D perovskite film with a composition of $Cs_{0.05}FA_{0.85}MA_{0.10}Pb(I_{0.90}Br_{0.10})_3$ was chosen and prepared according to the reported method.[30] The mixed perovskite film was deposited using a one-step method containing anti-solvent

treatment. During the anti-solvent process, Indigo was dissolved in chlorobenzene (CB) at optimal concentration to post-treat the 3D perovskite film *via* a dripping approach (see Experimental Section for details), followed by annealing at 100 ºC for 60 min. The concentrations of Indigo were optimized to be 0.05 mg/mL according to the statistical analysis of PCE (Table S1). To gain a fundamental understanding of the interactions between Indigo molecules and 3D mixed perovskite, the Fourier transform infrared (FTIR) spectroscopy and X-ray photoelectron spectroscope (XPS) were performed, respectively. As illustrated in **Figure 1b** (with the full regions shown in Figure S1), the characteristic peaks at around 1650 and 1370 cm^{-1} are attributed to the conjugated aromatic ring.[15, 25] More interestingly, the characteristic stretching vibration of the C=O in Indigo slightly shifts from 1630 cm^{-1} to ~1614 cm^{-1} and the stretching vibration intensity of -NH decreases upon deposition onto perovskite film, suggesting the chemical interaction between Indigo molecule and perovskite.[15, 18] More direct evidence about the interaction between Indigo molecule and perovskite surface is provided by the X-ray photoelectron spectroscopy (XPS) characterization (**Figure 1c-1d**). In comparison with the pristine perovskite film, the Indigo treated film exhibits shift to lower binding energy positions, suggesting the formation of chemical bonding between Indigo molecule and mixed perovskite.[30, 34] In specific, the characteristic peaks of Pb in the pristine thin film shows two peaks located at 142.21 and 137.26 eV, corresponding to the Pb $4f_{5/2}$ and Pb $4f_{7/2}$ core level, respectively (**Figure 1d**), and both peaks undergo ~0.40 eV shift to the lower binding energy position. Meanwhile, in the core level spectra of I, we observe the similar down shift after Indigo treatment. According to previous report, such a shift may be attributed to the coordination bonding between O and Pb *via* Lewis based-acid interaction between the C=O bond of Indigo with the Pb^{2+} in the thin film, and the interaction between -NH and perovskite surface (halide I^-) *via* hydrogen bonding.[37, 40] Based on these results, a schematic diagram of defect passivation mechanism for Indigo post-treatment is shown in **Figure 1e**.

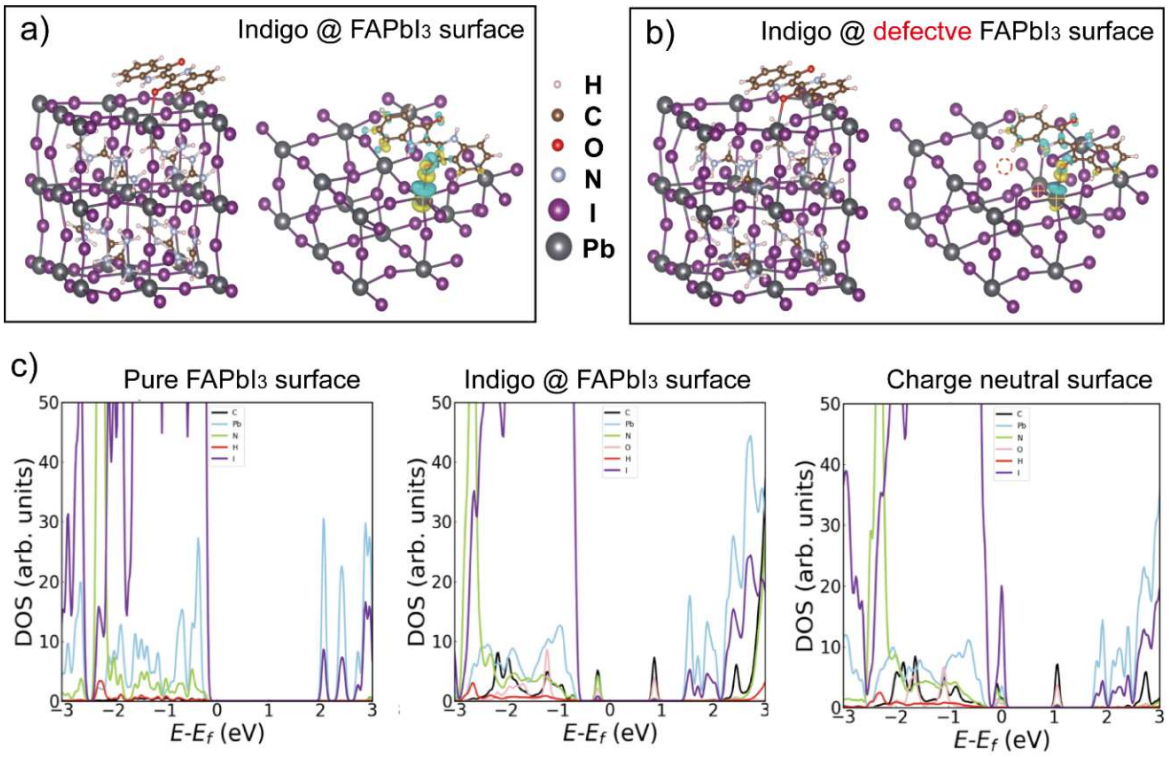

Figure 2. DFT calculated structure and charge density difference (CDD) for Indigo molecule docking on a) stoichiometric $FAPbI_3$ and b) defective $FAPbI_3$ surface containing neutral Pb vacancies (indicated with dotted lines in the figure), c) DFT calculated DOS for the relaxed: a) $FaPbI_3$ surface, b) Indigo@$FAPbI_3$, c) Indigo@$FAPb_{1-x}I_3$, the Fermi energy level has been shifted to 0 eV in all the cases.

To gain insight into the passivation mechanism and interaction between Indigo and perovskite surface, first-principles calculations based on density functional theory (DFT)[41] were carried out. The generalized gradient approximation (GGA)[42] in the flavour Perdew-Burke-Ernzerhof (PBE) was used to describe the effects of electronic exchange and correlation. The projector-augmented wave method (PAW)[43] was employed to represent the ionic cores. A 12-atom unit cell of $FAPbI_3$ was first relaxed with a Monkhorst-Pack k-point mesh of 8×8×8. Then, a 3×3×2 slab system reproducing the surface Miller index <001> of $FAPbI_3$ was generated by adding a vacuum region of 20 Å thickness, in which the Pb and I ions were exposed. Detailed calculation parameters can be found in the Supporting Information. The DFT calculations showed that the oxygen atoms in the Indigo molecule tend to form bonds with $FAPbI_3$ surface Pb^{2+}, as demonstrated by binding energy, charge density difference (CDD,

shown in **Figure 2a**) and Bader charge analysis. In particular, based on the bonding energy formula :

$$E_{binding} = E_{indigo@FAPb_{1-x}I_3} - E_{indigo} - E_{FAPb_{1-x}I_3 slab}$$

a large Indigo binding energy of -1.52 eV for a non-defective $FAPbI_3$ surface was estimated, which suggests chemical adsorption of the molecule on the perovskite surface. Reassuringly, CDD showed that charge is mostly transferred from $FAPbI_3$ surface Pb ions (e.g., Pb cross-labelled in Figure 2a) to the closest O atoms in the Indigo molecule (i.e., about 0.1 electrons according to Bader charge analysis). Then, the binding of Indigo molecules on defective $FAPbI_3$ surfaces containing neutral Pb vacancies was analyzed (**Figure 2b**). In this case, the binding energy of the Indigo molecule amounts to -1.58 eV, which indicates a slightly stronger adsorption on the perovskite surface than in the non-defective case. When Pb surface vacancies are created, $FAPbI_3$ surface I^- start to interact also significantly with the Indigo molecule. For instance, Bader charge analysis indicates that the I ion cross-labelled in **Figure 2b**, which is closest to the created Pb surface vacancy and O Indigo, donates about ~0.06 electrons to the molecule. In terms of the partial density of state (pDOS, **Figure 2c**), upon adsorption of the Indigo molecule on the $FAPbI_3$ surface it is appreciated the appearance of highly hybridized Indigo O, C, N, I and Pb electronic orbitals close to the Fermi energy level (**Figures 2c**), which is a clear signature of the formation of Perovskite-Indigo molecule chemical bonds. In the case of defective $FAPbI_3$ surfaces, large hybridizations between $FAPbI_3$ I and Indigo molecular orbitals appear close to the Fermi level (**Figure 2c**), which is consistent with the strengthening of the Perovskite-Indigo molecule interactions driven by the creation of Pb surface vacancies. Overall, theoretical DFT results appear to confirm that adsorption of Indigo molecules successfully passivates the $FAPbI_3$ surface by trapping the unpaired and delocalized electrons stemming from Pb surface ions and vacancies.

In order to further understand the Indigo treatment on the crystallization process and relevant thin film morphology, more measurements on the corresponding perovskite thin films were conducted. The effect of Indigo treatment on surface morphology and crystal structure properties of mixed perovskite film was first investigated by the scanning electron microscopy (SEM). Top-view SEM images of mixed perovskite film treated with pure CB, CB with Indigo at a concentration of 0.05 and 0.10 mg/mL are displayed in **Figure 3**. Pristine perovskite film shows a smooth morphology with apparent grain boundary. It is worth noting that the Indigo-treated perovskite film, displaying increased crystal domain size and more uniform size distribution than the control. The crystal grain further increases at higher Indigo loading while decreased uniformity. The similar result was found in the atomic force microscopy (AFM) characterization. As shown in **Figure 3d-3f**, both the surface roughness and the crystal domain size increase after the introduction of Indigo treatment. The larger and more uniform crystal grain size of the mixed perovskite film suggests few defects and non-radiative recombination centers, which is beneficial for achieving enhanced photovoltaic performance.[25, 44] To further verify the influence of Indigo on the crystallization of mixed perovskite film, 2D grazing incidence wide-angle X-ray scattering (GIWAXS) was conducted on the corresponding perovskite films.[30] As shown in **Figure 3g-3h**, after Indigo treatment, we observe a stronger preference for almost all the diffraction peaks of (100), (110), (200), (210), (211), and (220), especially in the out-of-plane direction. Meanwhile, the X-ray diffraction (XRD) measurement was also performed on FTO/c-TiO_2/$Cs_{0.05}FA_{0.85}MA_{0.10}Pb(I_{0.90}Br_{0.10})_3$ samples (Figure S2). All the films show typical patterns of a black perovskite crystal with characteristic diffraction peak at 13.9^o for the (110) phase.[30, 38] Besides, in compared with the pristine film, the Indigo-modified perovskite films exhibit enhanced diffraction intensity and decreased full width at half maximum (FWHM), indicating enhanced crystallinity.

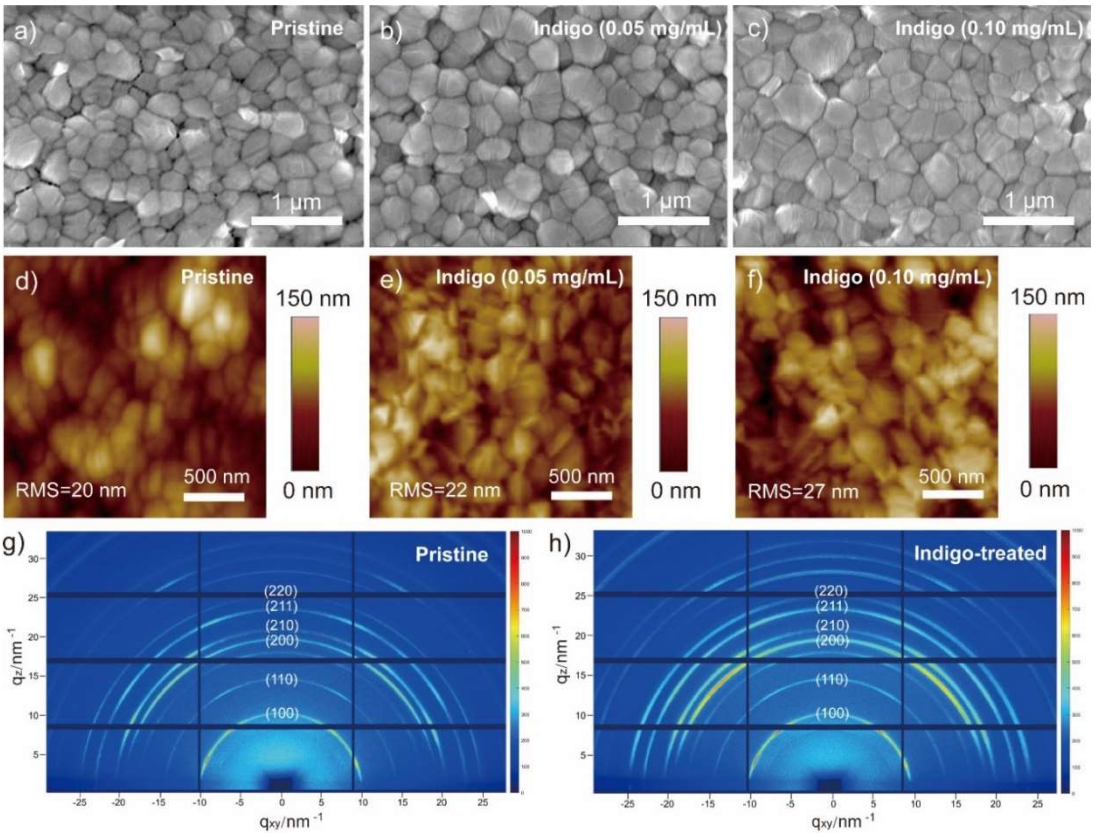

Figure 3. a)-c) Top-view SEM images, d)-f) AFM images and g)-h) 2D-GIWAXS patterns of pristine and Indigo-treated perovskite films.

To explore the effects of Indigo passivation on the charge dynamics of perovskites, we further performed steady-state photoluminescence (PL) and time-resolved photoluminescence (TRPL) measurements on different perovskite films deposited on the quartz substrates.[24, 34, 45] Due to the relatively low Indigo concentration (0.05 mg/mL), it is not surprising to find that the difference of optical absorption between pristine and indigo treated perovskite film is not significant (Figure S3). The Indigo treated perovskite film (0.05 mg/mL) exhibits significantly enhanced PL intensity and slightly blue shift compared to the control perovskite film (**Figure 4a**). Such a phenomenon is attributed to better passivated perovskite surface and a decrease of spontaneous radiative recombination induced by trap states.[23, 46-47] Further increasing Indigo concertation leading to decreased PL intensity (Figure S4), which may be attributed to the accumulation of the Indigo molecules.[48] Meanwhile, we also calculated the lifetime (Table S2) of charge carriers from the TRPL measurements (**Figure 4b**). The Indigo treated perovskite

film exhibits a longer average lifetimes (τ_{ave}) lifetime (455 ns for the 0.05 mg/mL) than the control one (300 ns), suggesting a higher quality film with suppressed trap-assisted non-radiative recombination.[49-50] In comparison with the conventional PL spectroscopy, 2D PL mapping imaging allows us to assess the uniformity of the perovskite film (**Figure 4c-4d**). More uniform intensity distribution was found in the Indigo treated perovskite film relative to the pristine one, which may result from the elimination of defects at both the surface and grain boundaries.[28, 46] To investigate the charge transfer dynamics in control and Indigo-treated perovskite films, femtosecond transient absorption (fs-TA) measurements were carried out to collect detailed information for both radiative and nonradiative processes. As shown in **Figure 4e-4f**, the Indigo-treated film prosses longer decay time associated with trap states relative to the control one, demonstrating improved charge separation in Indigo-treated films and suggesting that the organic small molecule Indigo can effectively passivate surface trap states and beneficial for reducing non-radiative recombination in perovskite thin film.[51] All these results confirmed that Indigo passivation can effectively passivate the perovskites, leading to better polycrystalline perovskite films with fewer trap states.

To understand the effect of the Indigo passivation on photovoltaic performance, we fabricated PSCs with a planar n-i-p structure of glass/fluorine-doped tin oxide (FTO)/TiO_2/ $Cs_{0.05}FA_{0.85}MA_{0.10}Pb(I_{0.90}Br_{0.10})_3$/Spiro-OMeTAD/$MoO_3$/Ag shown in **Figure 5a**. Each layer of the device can be clearly identified from the cross-sectional SEM image (**Figure 5b**). The optimization of Indigo concertation is shown in Tables S1. Indigo at a concentration of 0.05 mg/mL was found to be the optimal condition, which is in line with the above characterization. **Figure 5c** shows the current density versus voltage (*J-V*) curves of the optimal device with and without Indigo treatment, under 1.5G illumination at an intensity of 100 mW/cm^2, with the device parameters summarized in **Table 1**. The control device shows a best PCE of 20.18% with a J_{sc} of 24.15 mA/cm^2, a V_{oc} of 1.07 V, and an *FF* of 0.78, while the champion device

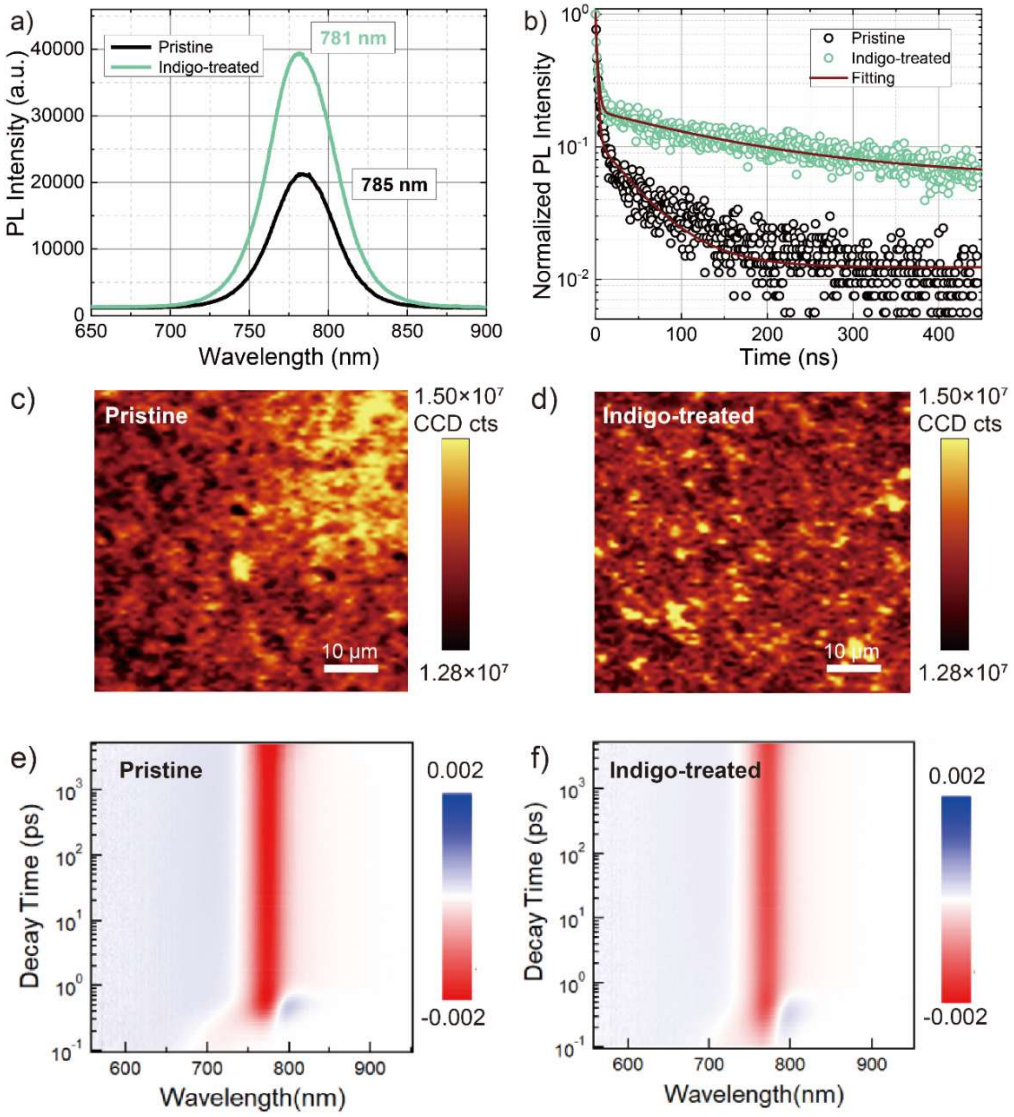

Figure 4. a) Steady-state PL spectra, b) TRPL decay spectra of the perovskite film, c)-d) normalized PL mapping of the pristine perovskite film and Indigo-treated perovskite film, e)-f) 2D time-wavelength-dependent TA color maps of pristine and Indigo-treated perovskite films.

after Indigo treatment delivers a significantly improved PCE up to 22.91% with an increased J_{sc} of 25.12 mA/cm^2, a V_{oc} of 1.14, and an *FF* of 0.80. In addition, as shown in **Figure 5d**, the control and Indigo-treated cells exhibit steady-state power outputs (SPO) at the maximum power point of 19.25% and 22.17%, respectively, confirming the reliability of PCE obtained from the *J-V* measurements. The PCE (**Figure 5e**) and other device parameters distribution statistics of 24 devices for each case further validates the significant enhancement of device performance and reproducibility. Moreover, the Indigo-treated device exhibits a reduced *J-V* hysteresis effect (hysteresis index = 0.034) relative to the control device (hysteresis index =

0.076). Meanwhile, the incident photon conversion efficiencies (IPCEs) of the control and Indigo-treated device were also recorded and the results are shown in **Figure 5f**, the Indigo-treated device exhibits higher values relative to the control device almost across the entire wavelength range (300-850 nm), suggesting better charge transport and carrier collection in device after Indigo passivation. The integrated current density values over the AM 1.5G solar spectrum for control and Indigo-treated cell are 22.38 mA/cm^2 and 23.52 mA/cm^2, respectively,

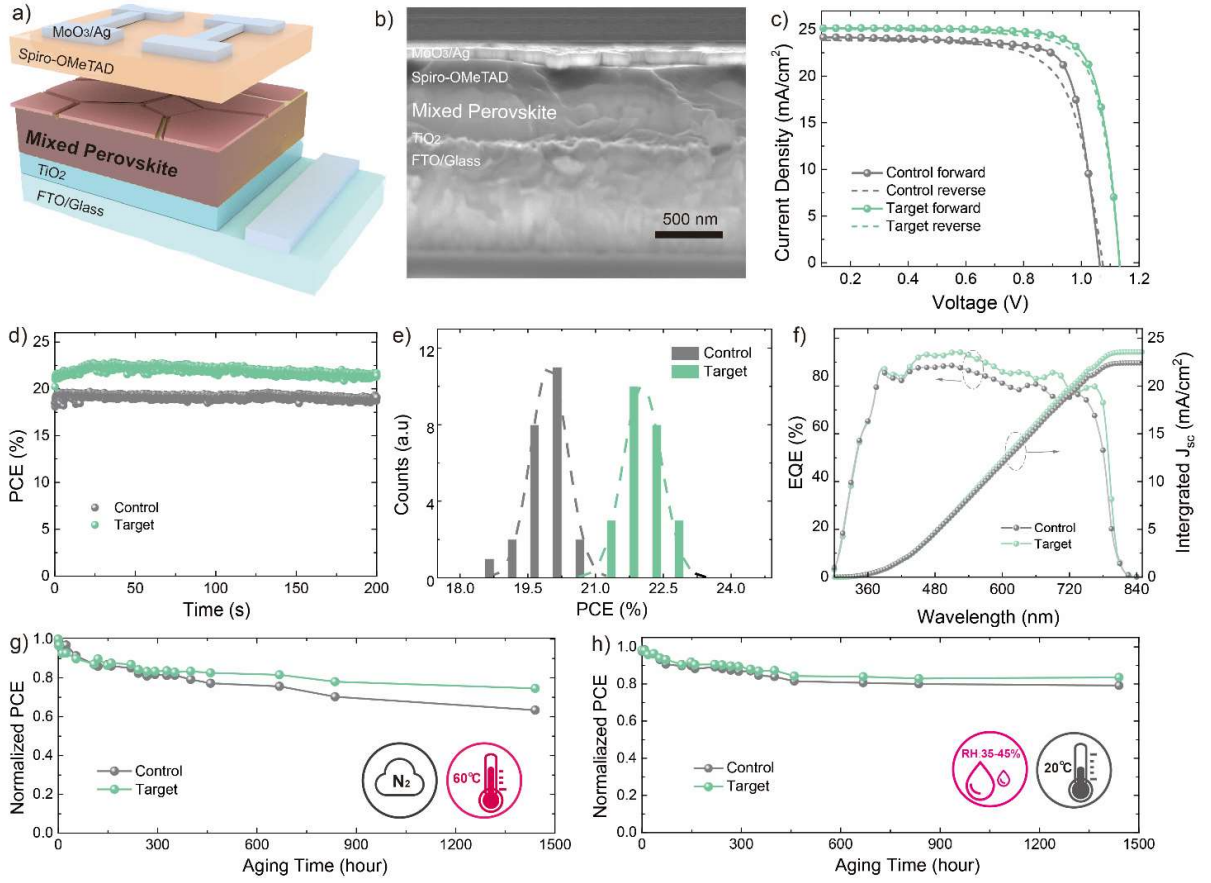

Figure 5. a) Device architecture of PSCs and b) their corresponding cross-sectional SEM image, the scale bar is 500 nm, c) *J-V* curves of the champion cells, d) stabilized power output of the champion Indigo-treated PSCs under maximum power point (MPP) tracking for 200 s, e) the PCE histogram of 24 devices, f) *J-V* curve of the champion cell of $Cs_{0.05}FA_{0.85}MA_{0.10}Pb(I_{0.90}Br_{0.10})_3$ PSCs, and the inset shows the corresponding EQE spectra, g) Long-term stability of unencapsulated Indigo-treated and Pristine devices under N_2 environment with continuous 60 ºC heating and shelf storage stability exposed in ambient environment (20 ºC, relative humidity of 35-45%).

in good agreement with the J_{sc} values obtained from the *J-V* curves. All these results demonstrate improved charge transport and less charge recombination in the device with Indigo passivation, which is beneficial for improving photovoltaic performance. In addition to the

enhancement of photovoltaic efficiency, the instability issue is a critical issue that hampers the further development of PSCs. Here, we evaluated the stability of unencapsulated devices under N_2 environment with continuous 60 °C heating and the shelf storage stability under ambient environment (20 °C, relative humidity of 35-45%) over 1500 hours.[52] It was found that over 75% of the PCE of the Indigo-treated PSCs can be maintained after thermal aging for 1500 hours, whereas the control PSCs show a PCE drop of ~40% for the same time. Moreover, the PCE of the control device drops by ~25% after 1500 h storage under ambient environment without any encapsulation, whereas the devices with Indigo passivation show a PCE drop of only ~15% for the same time, indicating the Indigo post-treatment improves the humidity stability of the PSCs (**Figure 5g-h**). The contact angle of water drop on control and the Indigo-treated film is presented in Figure S5, indicating a more hydrophobic nature after Indigo treatment, which is beneficial for preventing moisture invasion. The rich hydrogen bonds and carbonyl structures in the organic passivating agent can enhance device stability both in terms of humidity and thermal stress have been reported in recent work,[18, 37] herein, we present a simple yet efficient pathway using abundant and low-cost natural organic dyes to achieve high-performance perovskite solar cells.

Table 1. Photovoltaic parameters of the devices based on pristine and Indigo-treated perovskite thin film, the average values were summarized from 24 parallel devices.

Sample		V_{oc} (V)	J_{sc} (mA/cm^2)	FF	PCE (%)
Control	Forward	1.07	24.15	0.78	20.16
	Reserve	1.07	23.87	0.73	18.64
	Average	1.06±0.03	23.92±0.26	0.76±0.01	19.45±0.46
Indigo	Forward	1.14	25.12	0.80	22.91
	Reserve	1.14	25.21	0.77	22.13
	Average	1.12±0.01	24.87±0.31	0.79±0.01	22.00±0.53

Finally, we characterized the control and Indigo-treated solar cells to understand the kinetics behind enhanced device performance. The Space-charge-limited current (SCLC)

characterization was employed to study the defect density of perovskite films after Indigo passivation. The *J-V* curves of the hole-only device with a structure of glass/FTO/PEDOT:PSS/ Perovskite/Spiro-OMeTAD/MoO_3/Ag are shown in **Figure 6a**. The linear relation indicates an ohmic response of the device at the region of low bias voltage, while the current increased quickly as the voltage went up and exceeded the kink point, which signified the trap-states were fully filled.[24] And the trap-state density (n_t) can be calculated from the trap-filled limit voltage (V_{TFL}) using the equation:

$$n_t = \frac{2\varepsilon\varepsilon_0 V_{TFL}}{eL^2}$$

where ε is the relative dielectric constant of perovskite, ε_0 is the vacuum permittivity, and L is the thickness of the perovskite layer. The V_{TFL} of control and target device is 0.305 and 0.153 V, giving a corresponding n_t values of 1.20×10^{17} cm^{-3} and 6.02×10^{16} cm^{-3}, respectively. The lower value for the target device indicates that the hole trap state density of perovskite thin films was greatly reduced through Indigo passivation.[38] Moreover, the trap density of state (tDOS) in the device is also characterized by thermal admittance spectroscopy measurements (**Figure 6b)**. It is obvious that the trap density of target device is lower than that of control one at the shallow trap region. Meanwhile, The J_{sc} and V_{oc} as a function of illumination intensity was conducted. Figure S6 shows the values of the exponential factor (α) is 0.913 and 0.912 for the control and target devices, respectively, indicating both devices exhibit similar bimolecular recombination. For better comparison, the light intensity dependence on V_{oc} was also studied. If the slope is greater than 1kT/q (where k is the Boltzmann constant, T is the temperature, and q is the elementary charge), it indicates the interfacial trap-assisted Shockley−Read−Hall (SRH) recombination.[53] The slope of target device is 1.57 KT/q, which is lower than that of the control device (1.86 KT/q), indicating that a trap assisted SRH recombination process occurring at the charge collection interfaces has been effectively suppressed though the Indigo passivation (Figure S7). Furthermore, to fully understand the improvement of the V_{oc}, electrochemical

impedance spectroscopy (EIS) was utilized to study the charge-transfer resistance (R_{tr}) and recombination resistance (R_{rec}) in these devices. The Nyquist plots of the control target devices are shown in **Figure 6c**, with the parameters listed in Table S3. The Indigo treated target device shows a reduced R_{tr} (30.39 Ω) and an increased R_{rec} (267.2 Ω), indicating that Indigo passivation can suppress the carrier recombination and improve the charge transfer at the interface, which is consistent with the increased V_{oc} and J_{sc}. Similar conclusion can be found from the dark *J-V* characteristics (Figure S8), the leakage current for the target device is decreased compared to the that of the control one, suggesting suppressed interfacial recombination. In addition, Mott-Schottky analysis of the capacitance-voltage (C-V) curves was employed to investigate the built-in potential (V_{bi}) and the width of depletion region of control and target solar cells (Figure S9). the Indigo-treated device exhibits higher V_{bi} 0.958 V than the 0.924 V of pristine device, which indicates wider depletion layer to accelerate charge carrier separation and promote charge transport.[36, 46] Meanwhile, transient photovoltage (TPV) were performed on both devices（**Figure 6d**). The target device shows a photovoltage decay time of 3.97 μs, which is longer than 2.81 μs for the control device, suggesting that Indigo passivation can suppress non-radiation recombination and deliver a faster charge transport rate. All these results indicate the intrinsic mechanism of enhancement of photovoltaic performance lies in the improvement of the interfaces, which is attributed to the Indigo molecular passivation.

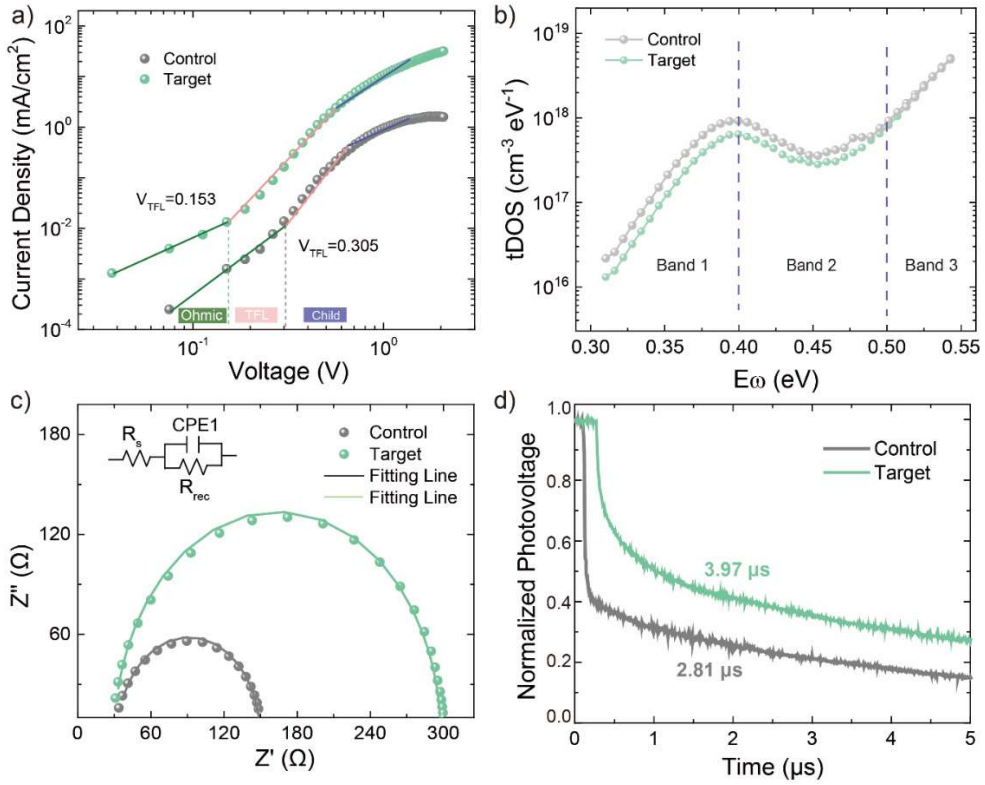

Figure 6. a) SCLC measurements of hole-only devices, b) The trap density (tDOS) of control and target device calculated from the frequency-dependent capacitance plot, c) Nyquist plots of the optimized Target and control devices, d) Transient photovoltage (TPV) decay spectroscopy pattern of the Indigo-treated and control devices.

3. Conclusion

In conclusion, we have demonstrated a new kind of Indigo molecular passivator for design and preparation of high-quality hybrid perovskite film for photovoltaic application. Through dissolving functional Indigo molecule in CB at optimal concertation to treat the spinning $Cs_{0.05}FA_{0.85}MA_{0.10}Pb(I_{0.90}Br_{0.10})_3$ perovskite film, we proved that the existence of the C=O/-NH systems is important to passivate for defects in pristine perovskite film. Combined theoretical and experimental results confirmed the strong interaction between Indigo and perovskite via Lewis base/acid coordination effectively reduce the surface defects of perovskite thin film and suppress the trap-assisted nonradiative recombination. Moreover, with the assistance of Indigo passivation, the resultant perovskite film displays better morphology with increased crystal domain size and more uniform size distribution than the pristine one. These superior merits enabled an excellent PCE of 22.91% for Indigo-treated PSCs with a negligible hysteresis, in

comparison to that of 20.12% in the control device. Furthermore, the carbonyl groups and hydrogen bonds structures in the Indigo dye can significantly enhance device stability both in terms of humidity and thermal stress. Combining the characteristics of the abundant nature available, low cost and multifunctional Lewis based groups of organic small molecular dye Indigo with emerging halide perovskite helps the commercialization and high performance of hybrid halide perovskite.

Experimental Section

Preparation and characterization of perovskite solar cells: Firstly, the fluorine-doped tin oxide (FTO) glass substrates were sequentially cleaned with detergent water, acetone and isopropanol for 1hour and then dried with N_2. Then the clean FTO as the substrate were used for deposition of titanium dioxide. After treated under ultraviolet light and ozone for about 15 min, the FTO glasses were immersing in 200 mL ultrapure water with 4.5 mL titanium tetrachloride for 60min at 70 ºC. Further, the FTO substrates coated with TiO_2 was washed by distilled water and then annealed at 180 ºC for 30 minutes. After treated by ultraviolet ozone (UVO) for 15 min, the structures were transferred into nitrogen glove box (O_2 and H_2O both bellow 2.0 ppm). For the deposition of perovskite thin films, a 30 μL 1.20 M $Cs_{0.05}FA_{0.85}MA_{0.10}Pb(I_{0.90}Br_{0.10})_3$ precursor solution was spin-coating onto the c-TiO_2 layer at the speed 1000 rpm for 10 s (acceleration rate at 200 rpm s^{-1}) and 4000 rpm for 20 s (acceleration rate at 2000 rpm s^{-1}). During the second stage of spin coating (high speed) process, the antisolvent which contains different concentrations of Indigo was dripped (at 8 s) onto the perovskite surface. Before depositing the perovskite layer, the glove box was purged in N_2 for minimizing solvent residues of CB. Next, the as-deposited perovskite films were annealed at 100 ºC for 60 min and the color of the films were converted from gold to black in this process. After cooling down the films to room temperature, the hole transport solution Spiro-OMeTAD (contains 90 mg Spiro-OMeTAD, 35.5 μL of a 520 mg/mL lithium bis (trifluoro-methylsuphonyl) imide in acetonitrile and 20.6 μL of

4-tert-butylpyridine in 1mL chlorobenzene) was spin-coated onto the perovskite/c-TiO_2/FTO substrate at 4000 rpm for 20 s to produce about 200 nm of hole transport layer. Finally, 8 nm MoO_3 and 120 nm Ag was deposited by thermal vacuum evaporation under 10^{-6} Torr. Also, the current density-voltage (*J-V*) characteristics of the solar cells was measured using a Keithley 2400 Digital Source Meter and simulated AM 1.5G spectrum at 100 mW/cm^2 with a solar simulator (Class AAA, 94023A-U, Newport) in the ambient atmosphere. Before test, the light intensity of the Xenon lamp was calibrated with a standard silicon solar cell (91150V, Newport Oriel). The active area of 7.25 mm^2 was defined by a shadow mask. The external quantum efficiency (EQE) measurement of the solar cells was characterized on a Solar Cell Scan 100 system (Zolix Instruments Co. Ltd.).

Supporting Information

Supporting Information is available from the Wiley Online Library or from the author.

Acknowledgements

This work was supported by the National Key Research and Development Program of China (2019YFE0108600), National Natural Science Foundation of China (52073198, 22161142003 and 61911530158), Natural Science Foundation of Jiangsu Province (BK20211598), Science and Technology Program of Jiangsu Province (BZ2020011), Science and Technology Program of Suzhou (SYG202037), "111" project, the China Postdoctoral Science Foundation (Grant No. 2021T140495), Collaborative Innovation Center of Suzhou Nano Science and Technology, Soochow University.

Received: ((will be filled in by the editorial staff))
Revised: ((will be filled in by the editorial staff))
Published online: ((will be filled in by the editorial staff))

References

[1] N. J. Jeon, J. H. Noh, Y. C. Kim, W. S. Yang, S. Ryu, S. I. Seok, *Nat. Mater.* **2014**, 13, 897.

[2] H. Zhou, Q. Chen, G. Li, S. Luo, T. B. Song, H. S. Duan, Z. Hong, J. You, Y. Liu, Y. Yang, *Science* **2014**, 345, 542.

[3] G. Kim, H. Min, K. S. Lee, D. Y. Lee, S. M. Yoon, S. I. Seok, *Science* **2020**, 370, 108.

[4] H. Lu, Y. Liu, P. Ahlawat, A. Mishra, W. R. Tress, F. T. Eickemeyer, Y. Yang, F. Fu, Z. Wang, C. E. Avalos, B. I. Carlsen, A. Agarwalla, X. Zhang, X. Li, Y. Zhan, S. M. Zakeeruddin, L. Emsley, U. Rothlisberger, L. Zheng, A. Hagfeldt, M. Gratzel, *Science* **2020**, 370.

[5] H. Min, M. Kim, S. U. Lee, H. Kim, G. Kim, K. Choi, J. H. Lee, S. I. Seok, *Science* **2019**, 366, 749.

[6] J. J. Yoo, G. Seo, M. R. Chua, T. G. Park, Y. Lu, F. Rotermund, Y. K. Kim, C. S. Moon, N. J. Jeon, J. P. Correa-Baena, V. Bulovic, S. S. Shin, M. G. Bawendi, J. Seo, *Nature* **2021**, 590, 587.

[7] M. Jeong, I. W. Choi, E. M. Go, Y. Cho, M. Kim, B. Lee, S. Jeong, Y. Jo, H. W. Choi, J. Lee, J. H. Bae, S. K. Kwak, D. S. Kim, C. Yang, *Science* **2020**, 369, 1615.

[8] H. Min, D. Y. Lee, J. Kim, G. Kim, K. S. Lee, J. Kim, M. J. Paik, Y. K. Kim, K. S. Kim, M. G. Kim, T. J. Shin, S. Il Seok, *Nature* **2021**, 598, 444.

[9] J. Sun, F. Li, J. Yuan, W. Ma, *Small Methods* **2021**, 5.

[10] M. Kim, G.-H. Kim, T. K. Lee, I. W. Choi, H. W. Choi, Y. Jo, Y. J. Yoon, J. W. Kim, J. Lee, D. Huh, H. Lee, S. K. Kwak, J. Y. Kim, D. S. Kim, *Joule* **2019**, 3, 2179.

[11] X. Zheng, B. Chen, J. Dai, Y. Fang, Y. Bai, Y. Lin, H. Wei, Xiao C. Zeng, J. Huang, *Nat. Energy* **2017**, 2.

[12] S. Yang, S. Chen, E. Mosconi, Y. Fang, X. Xiao, C. Wang, Y. Zhou, Z. Yu, J. Zhao, Y. Gao, F. De Angelis, J. Huang, *Science* **2019**, 365, 473.

[13] Q. Yang, X. Liu, S. Yu, Z. Feng, L. Liang, W. Qin, Y. Wang, X. Hu, S. Chen, Z. Feng, G. Hou, K. Wu, X. Guo, C. Li, *Energy Environ. Sci.* **2021**, DOI: 10.1039/d1ee02248b.

[14] Y. Zhang, Y. Wang, L. Zhao, X. Yang, C.-H. Hou, J. Wu, R. Su, S. Jia, J.-J. Shyue, D. Luo, P. Chen, M. Yu, Q. Li, L. Li, Q. Gong, R. Zhu, *Energy Environ. Sci.* **2021**, DOI: 10.1039/d1ee02287c.

[15] R. Wang, J. Xue, K. L. Wang, Z. K. Wang, Y. Luo, D. Fenning, G. Xu, S. Nuryyeva, T. Huang, Y. Zhao, J. L. Yang, J. Zhu, M. Wang, S. Tan, I. Yavuz, K. N. Houk, Y. Yang, *Science* **2019**, 366, 1509.

[16] Y. An, J. Hidalgo, C. A. R. Perini, A. F. Castro-Mendez, J. N. Vagott, K. Bairley, S. R. Wang, X. G. Li, J. P. Correa-Baena, *Acs Energy Lett* **2021**, 6, 1942.

[17] J. B. Li, R. Munir, Y. Y. Fan, T. Q. Niu, Y. C. Liu, Y. F. Zhong, Z. Yang, Y. S. Tian, B. Liu, J. Sun, D. M. Smilgies, S. Thoroddsen, A. Amassian, K. Zhao, S. Z. Liu, *Joule* **2018**, 2, 1313.

[18] P. Y. Liu, H. M. Xiang, W. Wang, R. Ran, W. Zhou, Z. P. Shao, *J Energy Chem* **2021**, 62, 243.

[19] S. W. Kim, G. Kim, C. S. Moon, T. Y. Yang, J. Seo, *Small Methods* **2021**, 5.

[20] X. Y. Yang, Y. Ni, Y. Z. Zhang, Y. J. Wang, W. Q. Yang, D. Y. Luo, Y. G. Tu, Q. H. Gong, H. F. Yu, R. Zhu, *ACS Energy Lett* **2021**, 6, 2404.

[21] M. J. Jeong, K. M. Yeom, S. J. Kim, E. H. Jung, J. H. Noh, *Energy Environ. Sci.* **2021**, 14, 2419.

[22] Y. Cai, J. Cui, M. Chen, M. M. Zhang, Y. Han, F. Qian, H. Zhao, S. M. Yang, Z. Yang, H. T. Bian, T. Wang, K. P. Guo, M. L. Cai, S. Y. Dai, Z. K. Liu, S. Z. Liu, *Adv. Funct. Mater.* **2021**, 31.

[23] L. Wen, Y. Rao, M. Zhu, R. Li, J. Zhan, L. Zhang, L. Wang, M. Li, S. Pang, Z. Zhou,

Angew. Chem. Int. Ed. **2021**, 60, 17356.
[24] Q. He, M. Worku, H. Liu, E. Lochner, A. J. Robb, S. Lteif, J. S. R. Vellore Winfred, K. Hanson, J. B. Schlenoff, B. J. Kim, B. Ma, *Angew. Chem. Int. Ed.* **2021**, 60, 2485.
[25] Y. Li, J. Shi, J. Zheng, J. Bing, J. Yuan, Y. Cho, S. Tang, M. Zhang, Y. Yao, C. F. J. Lau, D. S. Lee, C. Liao, M. A. Green, S. Huang, W. Ma, A. W. Y. Ho-Baillie, *Adv. Sci.* **2020**, 7, 1903368.
[26] S. Chen, X. Xiao, B. Chen, L. L. Kelly, J. Zhao, Y. Lin, M. F. Toney, J. Huang, *Sci. Adv.* **2021**, 7.
[27] Y. H. Chen, S. Q. Tan, N. X. Li, B. L. Huang, X. X. Niu, L. Li, M. Z. Sun, Y. Zhang, X. Zhang, C. Zhu, N. Yang, H. C. Zai, Y. L. Wu, S. Ma, Y. Bai, Q. Chen, F. Xiao, K. W. Sun, H. P. Zhou, *Joule* **2020**, 4, 1961.
[28] X. Zhu, M. Du, J. Feng, H. Wang, Z. Xu, L. Wang, S. Zuo, C. Wang, Z. Wang, C. Zhang, X. Ren, S. Priya, D. Yang, S. F. Liu, *Angew. Chem. Int. Ed.* **2021**, 60, 4238.
[29] J. Zhu, S. Park, O. Y. Gong, C. Sohn, Z. Li, Z. Zhang, B. Jo, W. Kim, G. S. Han, D. H. Kim, T. K. Ahn, J. Lee, H. S. Jung, *Energy Environ. Sci.* **2021**, 14, 4903.
[30] J. G. Sun, X. L. Zhang, X. F. Ling, Y. G. Yang, Y. Wang, J. J. Guo, S. Z. Liu, J. Y. Yuan, W. L. Ma, *J. Mater. Chem. A* **2021**, DOI: 10.1039/d1ta06514a.
[31] X. Zhao, T. Liu, A. B. Kaplan, C. Yao, Y. L. Loo, *Nano Lett.* **2020**, 20, 8880.
[32] Q. Hu, W. Chen, W. Q. Yang, Y. Li, Y. C. Zhou, B. W. Larson, J. C. Johnson, Y. H. Lu, W. K. Zhong, J. Q. Xu, L. Klivansky, C. Wang, M. Salmeron, A. B. Djurisic, F. Liu, Z. B. He, R. Zhu, T. P. Russell, *Joule* **2020**, 4, 1575.
[33] A. D. Taylor, Q. Sun, K. P. Goetz, Q. An, T. Schramm, Y. Hofstetter, M. Litterst, F. Paulus, Y. Vaynzof, *Nat. Commun.* **2021**, 12, 1878.
[34] F. Li, J. Yuan, X. Ling, Y. Zhang, Y. Yang, S. H. Cheung, C. H. Y. Ho, X. Gao, W. Ma, *Adv. Funct. Mater.* **2018**, 28.
[35] F. Cheng, R. He, S. Nie, C. Zhang, J. Yin, J. Li, N. Zheng, B. Wu, *J. Am. Chem. Soc.* **2021**, 143, 5855.
[36] R. Chen, Y. Wang, S. Nie, H. Shen, Y. Hui, J. Peng, B. Wu, J. Yin, J. Li, N. Zheng, *J. Am. Chem. Soc.* **2021**, 143, 10624.
[37] L. Yang, Q. Xiong, Y. Li, P. Gao, B. Xu, H. Lin, X. Li, T. Miyasaka, *J. Mater. Chem. A* **2021**, 9, 1574.
[38] Z. Zhang, Y. Gao, Z. Li, L. Qiao, Q. Xiong, L. Deng, Z. Zhang, R. Long, Q. Zhou, Y. Du, Z. Lan, Y. Zhao, C. Li, K. Mullen, P. Gao, *Adv. Mater.* **2021**, 33, e2008405.
[39] S. Li, Z.Yuan, J. Yuan, P. Deng, Q. Zhang, B. Sun, *J. Mater. Chem. A* **2014**, 2, 5427.
[40] S. S. Wang, Z. P. Zhang, Z. K. Tang, C. L. Su, W. Huang, Y. Li, G. C. Xing, *Nano Energy* **2021**, 82.
[41] C. Cazorla, J. Boronat, *Rev. Mod. Phys.* **2017**, 89.
[42] J. P. Perdew, K. Burke, M. Ernzerhof, *Phys. Rev. Lett.* **1996**, 77, 3865.
[43] P. E. Blochl, *Phys Rev B Condens Matter* **1994**, 50, 17953.
[44] Y. Xiao, W. Zheng, B. Yuan, C. Wen, M. Lanza, *Cryst. Res. Technol.* **2021**, 56.
[45] Y. W. Jang, S. Lee, K. M. Yeom, K. Jeong, K. Choi, M. Choi, J. H. Noh, *Nat. Energy* **2021**, 6, 63.
[46] Q. Zhou, Y. Gao, C. Cai, Z. Zhang, J. Xu, Z. Yuan, P. Gao, *Angew. Chem. Int. Ed.* **2021**, 60, 8303.
[47] J. Yuan, X. Zhang, Y. Qian, S. M. Zakeeruddin, B. W. Larson, Q. Zhao, J. Shi, J. Yang, K. Ji, Y. Zhang, Y. Wang, C. Zhang, S. Duhm, J. M. Luther, M. Gratzel, W. Ma, *Adv. Mater.* **2020**, 32, e2001906.
[48] M. Yang, T. Tian, W. Feng, L. Wang, W.-Q. Wu, *Acc. Mater. Res.* **2021**, DOI: 10.1021/accountsmr.1c00099.
[49] X. Ling, H. Zhu, W. Xu, C. Liu, L. Pan, D. Ren, J. Yuan, B. W. Larson, C. Grätzel, A. R. Kirmani, O. Ouellette, A. Krishna, J. Sun, C. Zhang, Y. Li, S. M. Zakeeruddin, J. Gao,

Y. Liu, J. R. Durrant, J. M. Luther, W. Ma, M. Grätzel, *Angew. Chem. Int. Ed.* **2021**, DOI: 10.1002/anie.202112555.
[50] Y. Zhang, Y. Li, L. Zhang, H. Hu, Z. Tang, B. Xu, N. G. Park, *Adv. Energy Mater.* **2021**, DOI: 10.1002/aenm.202102538.
[51] L. Hu, Q. Zhao, S. Huang, J. Zheng, X. Guan, R. Patterson, J. Kim, L. Shi, C. H. Lin, Q. Lei, D. Chu, W. Tao, S. Cheong, R. D. Tilley, A. W. Y. Ho-Baillie, J. M. Luther, J. Yuan, T. Wu, *Nat. Commun.* **2021**, 12, 466.
[52] E. Ochoa-Martinez, J. V. Milic, *Nat. Energy* **2021**, 6, 858.
[53] C. Zhang, H. Wang, H. Li, Q. Zhuang, C. Gong, X. Hu, W. Cai, S. Zhao, J. Chen, Z. Zang, *J Energy Chem* **2021**, DOI: 10.1016/j.jechem.2021.07.011.

We first demonstrate natural organic dye Indigo as a low-cost and highly efficient molecular passivator for high performance perovskite solar cells, and the Indigo passivation can boost power conversion efficiency of device to approaching 23% as well as enhanced device stability both in terms of humidity and thermal stress.

Keywords: Indigo, perovskite solar cells, passivation, natural dye, long-term stability.

Junjun Guo, Jianguo Sun, Shiwen Fang, Xufeng Ling, Xuliang Zhang, Yao Wang, Hehe Huang, Chenxu Han, Long Hu, Zizhen Zhou, Claudio Cazorla, Dewei Chu, Tom Wu, Jianyu Yuan, Wanli Ma**

Indigo: A Natural Molecular Passivator for Efficient Perovskite Solar Cells

ToC:

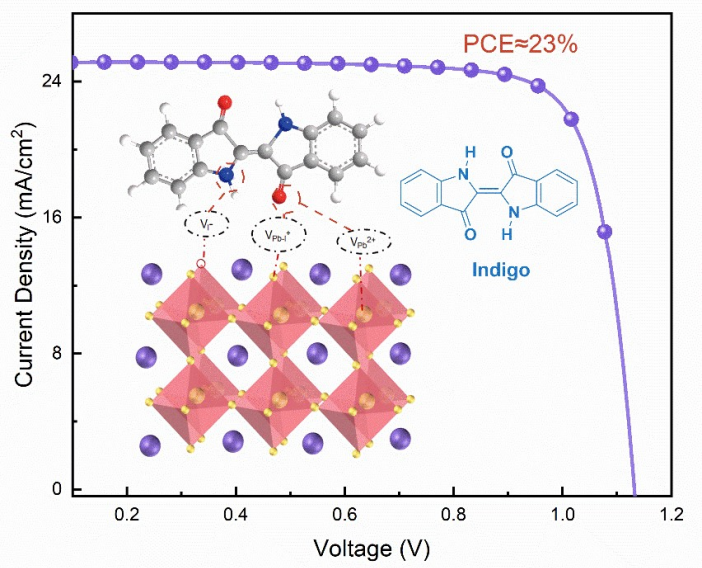

Supporting Information

Indigo: A Natural Molecular Passivator for Efficient Perovskite Solar Cells

Junjun Guo, Jianguo Sun, Shiwen Fang, Xufeng Ling, Xuliang Zhang, Yao Wang, Hehe Huang, Chenxu Han, Long Hu, Zizhen Zhou, Claudio Cazorla, Dewei Chu, Tom Wu, Jianyu Yuan, Wanli Ma**

J. Guo, J. Sun, S. Fang, X. Ling, Y. Wang, H. Huang, C. Han, Prof. J. Yuan, Prof. W. Ma
Institute of Functional Nano & Soft Materials (FUNSOM), Jiangsu Key Laboratory for Carbon-Based Functional Materials & Devices, Soochow University, 199 Ren-Ai Road, Suzhou Industrial Park, Suzhou, Jiangsu 215123, P. R. China.
E-mail: jyyuan@suda.edu.cn (J. Y.), wlma@suda.edu.cn (W. M.)

L. Hu
School of Engineering, Macquarie University, Sydney, New South Wales 2109, Australia.

Z. Zhou, Prof. D. Chu, Prof. T. Wu
School of Materials Science and Engineering, University of New South Wales (UNSW), Sydney, NSW 2052, Australia.

Prof. C. Cazorla
Departament de Física, Universitat Politècnica de Catalunya, Campus Nord B4-B5, E-08034 Barcelona, Spain

Materials

All the materials were mentioned is purchased from Greater solar, Alfa Aesar, Sigma-Aldrich or Xi'an Polymer Light Technology Corp. In detail, lead iodide (PbI2, 99.999%) from Sigma-Aldrich, lead bromide ($PbBr_2$, 99.99%) and cesium iodide (CsI, 99.99%) from Alfa Aesar and FAI and methylammonium bromide (MABr, 99.99%) from Great solar, Spiro-OMeTAD [2,2',7,7'-tetrakis-(N,N-dipmethoxyphenylamine)-9,9'-spiro-bifluorene] from Xi'an Polymer Light Technology Corp. Solvents used for perovskite solar cell include anhydrous N,N-dimethylformamide (DMF) and dimethyl sulfoxide (DMSO) from Alfa Aesar, the chlorobenzene used for antisolvent process were purchase from Sigma-Aldrich. All other chemicals were used as received without any further purification. More specifically, the 1 mL precursor (DMF:DMSO=4:1) contains 1.2 M perovskite and the perovskite thin film were made by the composition of mixed halides $Cs_{0.05}FA_{0.85}MA_{0.10}Pb(I_{0.90}Br_{0.10})_3$.

Characterization

Top-view and cross-section SEM images were obtained by a Zeiss Supra 55 field in high vacuum mode at 15 kV accelerating voltage. AFM images (tapping mode) were captured through an Asylum Research Cypher S AFM microscope. UV-Vis spectra were recorded on a PerkinElmer model Lambda 750. The steady-state and time-resolved PL spectra were recorded with a FluoroMax-4 spectrofluorometer excited at 460nm(HORIBA Scientific). GIWAXS measurements were performed at the Shanghai Synchrotron Radiation Facility Laboratory on Beamline BL14B1 using X-rays with a wavelength of λ= ~1.24 Å. The XPS spectra were obtained using a Kratos AXIS Ultra DLD ultrahigh vacuum photoemission spectroscopy system, with an Al Ka radiation source. And the FTO/c-TiO_2/ $Cs_{0.05}FA_{0.85}MA_{0.10}Pb(I_{0.90}Br_{0.10})_3$ perovskite/ Spiro-OMeTAD/MoO_3/Ag structure was adopted to fulfill this measurement EIS measurements carried out through Zahner IM6 electrochemical workstation while applying a

bias of under open-circuit with a frequency between 0.25 MHz and 0.05 Hz under a monochromatic LED (500 nm, 100 mW) light irradiation.

The computational method of first-principles calculations based on density functional theory (DFT)

The projector-augmented wave method (PAW) was employed to represent the ionic cores and the following electronic states were considered as valence: Pb 6p and 5d; I 4d 5s and 5p; C 2s and 2P; O 2s and 2p; H 1s; N 2s and 2p. A 1×1×1 Gamma k-point grid was employed for the slab calculations due to the large computational cost involved. The geometry optimizations were halted when the forces in the atoms were all below 0.05 eV/Å. The binding energy associated with Indigo docking on $FAPbI_3$ ($E_{binding}$) was calculated with the formula:

$$E_{binding} = E_{indigo@FAPb_{1-x}I_3} - E_{indigo} - E_{FAPb_{1-x}I_3 slab}$$

where $E_{indigo@FAPb_{1-x}I_3}$, E_{indigo} and $E_{FAPb_{1-x}I_3 slab}$ stand for the ground-state energy of the defective/non-defective indigo@$FAPbI_3$ system, Indigo molecular and defective/non-defective $FAPbI_3$ slab.

The charge density difference distribution is defined as:

$$\Delta\rho = \rho_{indigo@FAPb_{1-x}I_3} - \rho_{indigo} - \rho_{FAPb_{1-x}I_3 slab}$$

where $\rho_{indigo@FAPb_{1-x}I_3}$ is the total charge density of the defective/non-defective indigo@FAPbI3 slab system, and $\rho_{FAPb_{1-x}I_3}$ and ρ_{indigo} are the charge densities of the defective/non-defective $FAPbI_3$ slab and Indigo molecule by separate.

The calculation of TRPL fitting:

The test results of TRPL were fitted by a biexponential function as follows:

$$f(t) = A_1 e^{(-\frac{t}{\tau_1})} + A_2 e^{(-\frac{t}{\tau_2})} + A_0$$

where A_0 is a constant, t is the time, A_1 and A_2 are the decay amplitudes, τ_1 and τ_2 is the decay times, and the average PL lifetime (τ_{ave}) can be obtained by the equation as follows:

$$\tau_{ave} = \frac{A_1\tau_1^2 + A_2\tau_2^2}{A_1\tau_1 + A_2\tau_2}$$

The hysteresis index calculation

The hysteresis index of target and control device were calculated by a function as follows:

$$H = \frac{PCE_{reverse} - PCE_{forward}}{PCE_{reverse}}$$

SCLC measurements

A structure of Glass/FTO/PEDOT:PSS (ca. 30 nm)/perovskite (ca. 400 nm)/Spiro-OMeTAD (ca. 80 nm)/Ag (ca. 80 nm) was applied. The trap-state density (N_{trap}) of the QD film can be calculated by the equation:

$$N_{trap} = \frac{2\varepsilon_0\varepsilon_r V_{TFL}}{qL^2}$$

where ε_0 is the vacuum dielectric constant, ε_r is the relative dielectric constant of perovskite about 25, V_{TFL} represents the trap-filled limit voltage, q is the elemental charge and L is the distance between the electrodes.

tDOS measurements

The energetic profile of trap density of states (tDOS) can be derived from the angular frequency dependent capacitance using the equation:

$$N_T(E_\omega) = -\frac{V_{bi}}{qW}\frac{dC}{d\omega}\frac{\omega}{k_B T}$$

where C is the capacitance, ω is the angular frequency, q is the elementary charge, k_B is the Boltzmann's constant and T is the temperature. V_{bi} and W are the built-in potential and depletion width, respectively, which were extracted from the Mott–Schottky analysis. The applied angular frequency ω defines anenergetic demarcation, where ω_0 is the attempt-to-escape frequency.

$$E_\omega = k_B T ln \frac{\omega_0}{\omega}$$

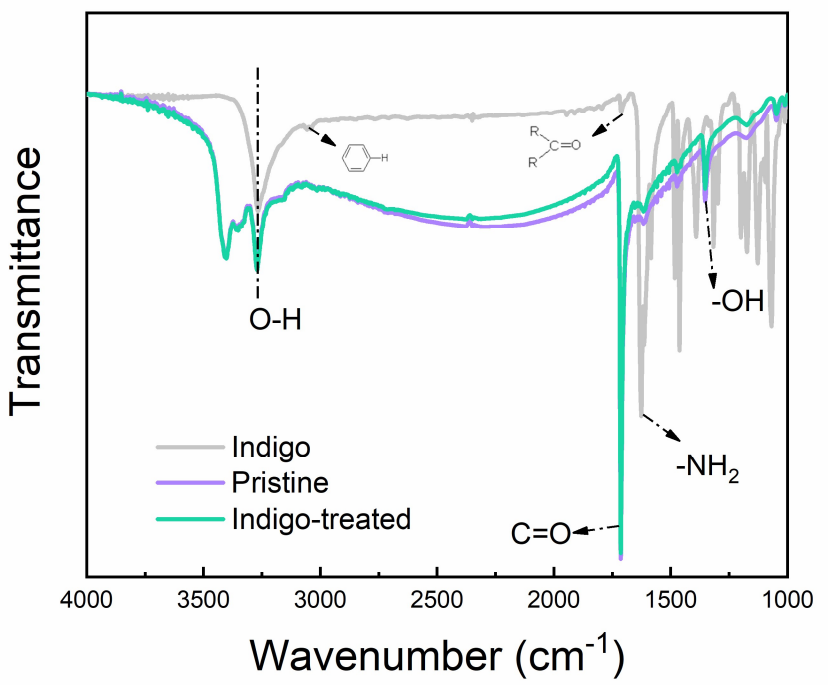

Figure S1. The FTIR spectra of Indigo, pristine, and Indigo-treated perovskites.

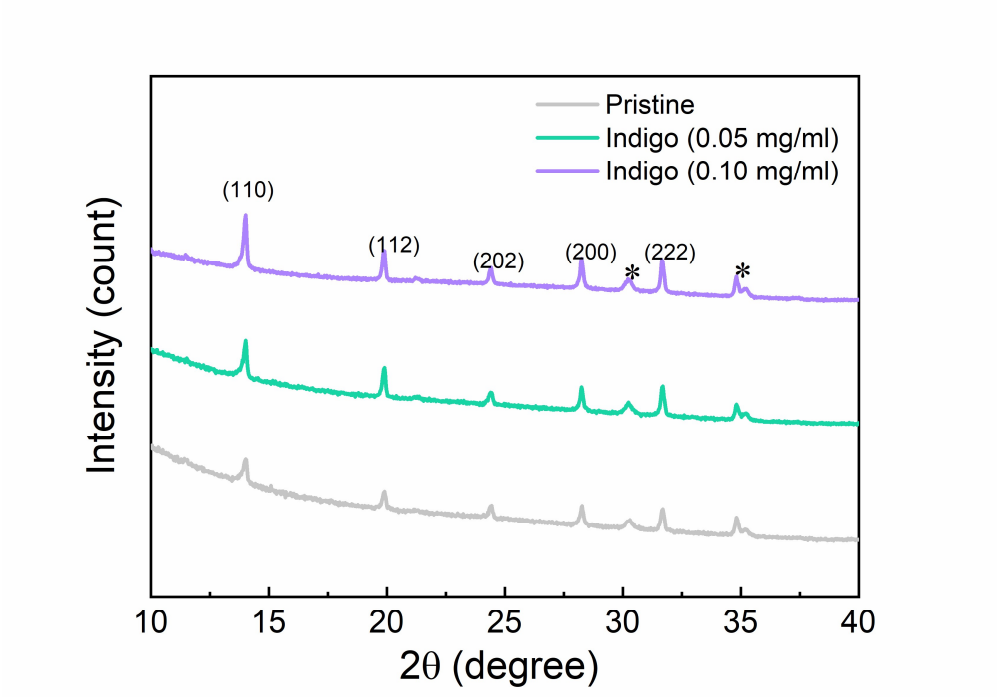

Figure S2. The XRD patterns and of the pristine and different concentration Indigo-treated perovskite thin films.

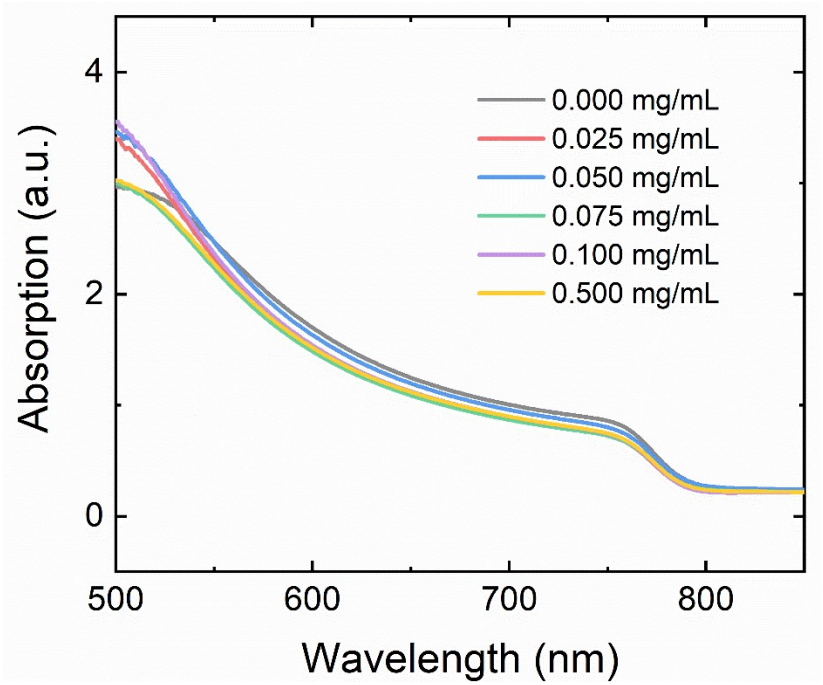

Figure S3. The Absorption of difference concentration Indigo-treated perovskite thin film.

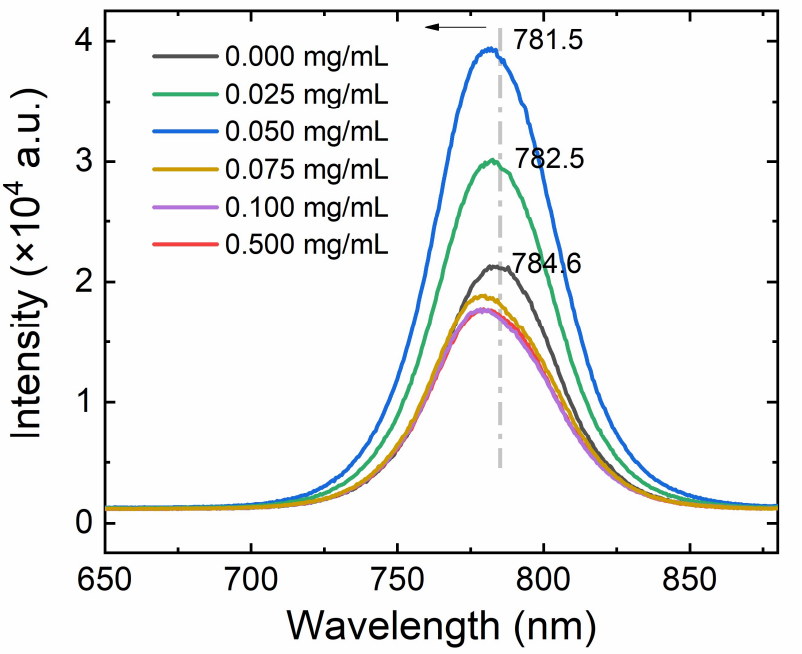

Figure S4. The Intensity of difference concentration Indigo-treated perovskite thin film.

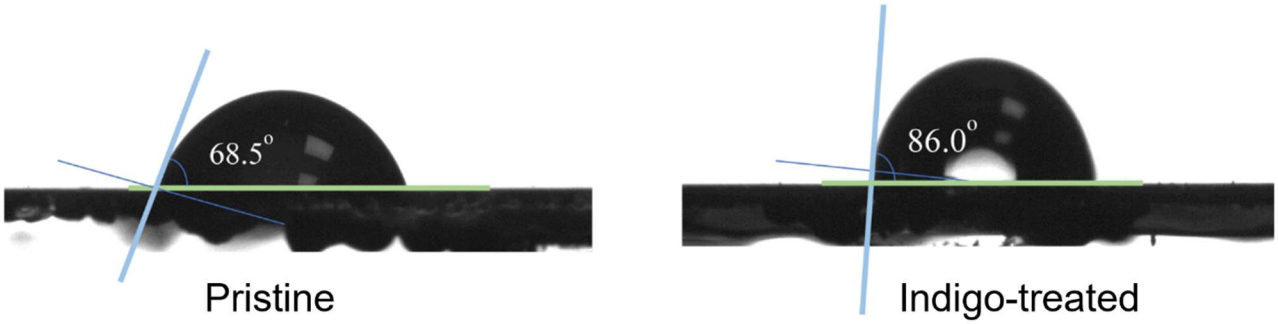

Figure S5. The contact angle of water drop on control and the Indigo-treated film.

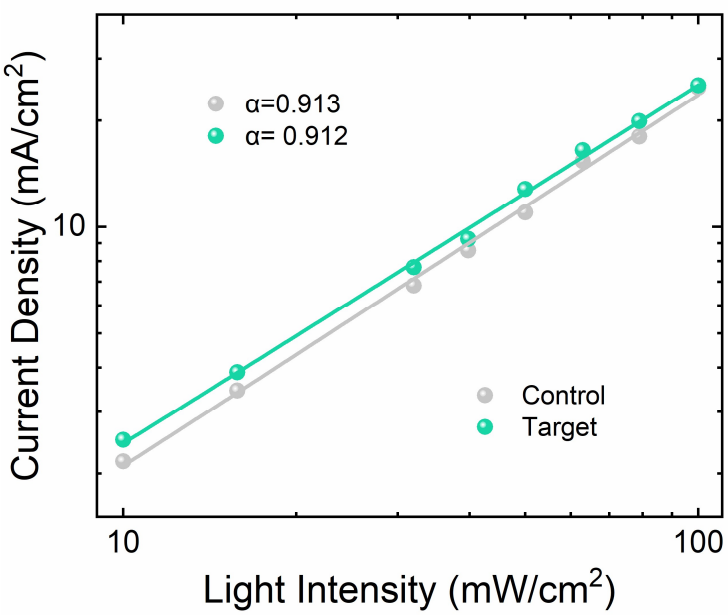

Figure S6. The relationship of J_{sc} with respect to light intensity for the control and target perovskite device.

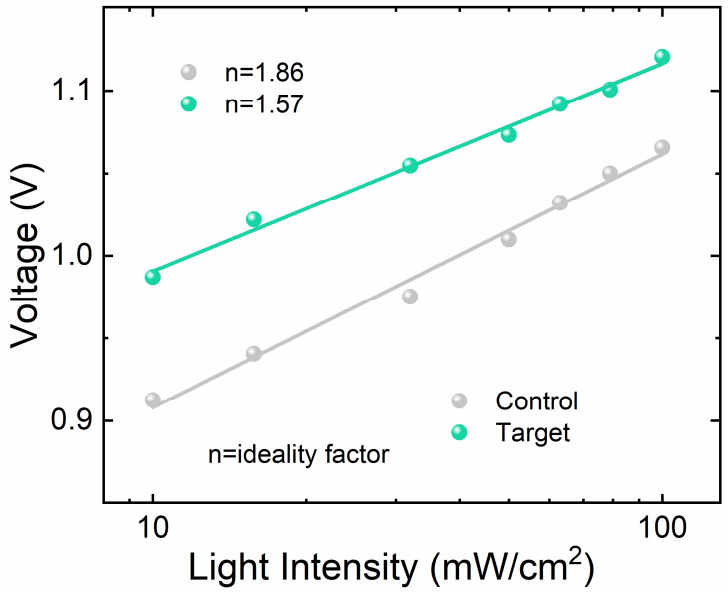

Figure S7. The light intensity dependence of V_{oc} of the mixed perovskite devices.

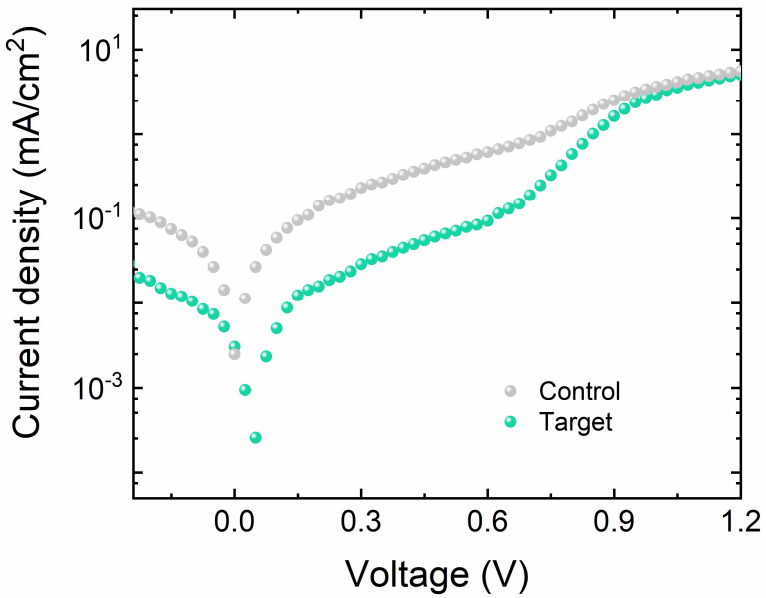

Figure S8. The dark-current pattern of the pristine and Indigo-treated perovskite thin films.

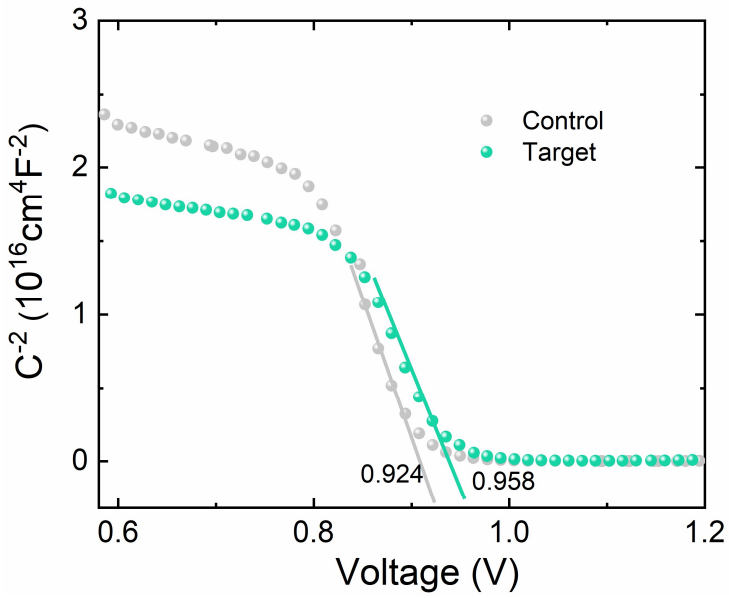

Figure S9. The Voltage dependence of capacitance of the mixed perovskite devices.

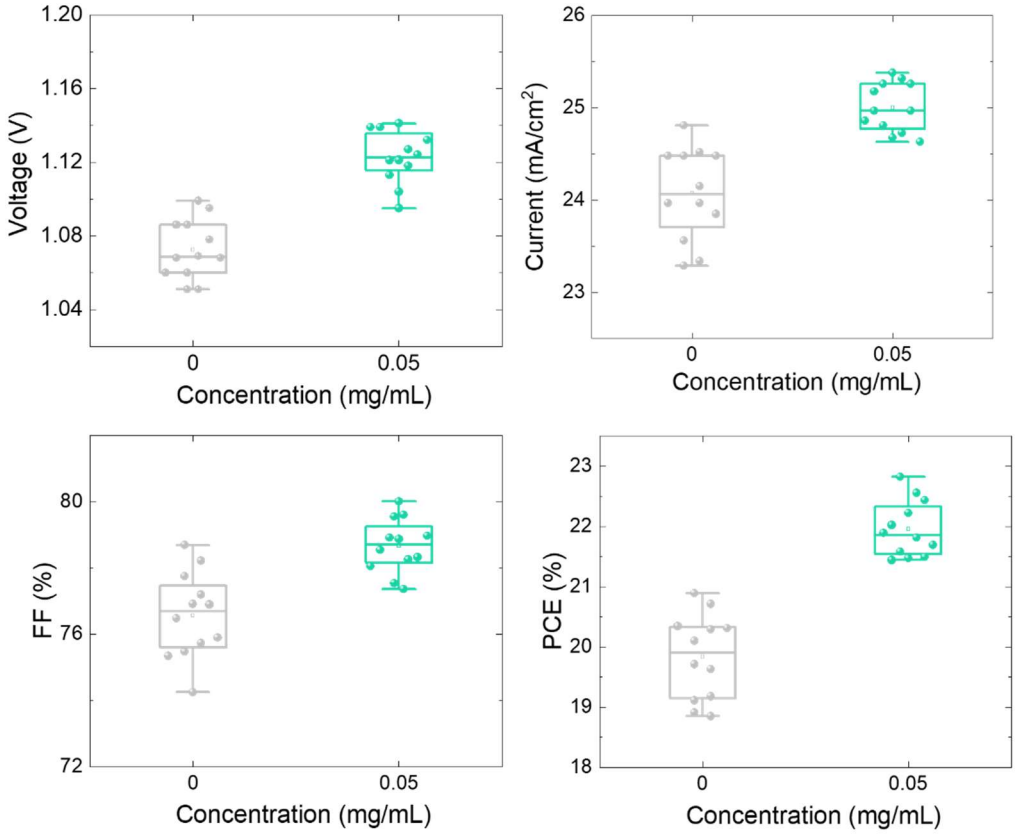

Figure S10. The statistical distribution of J_{sc}, V_{oc}, FF, and PCE for the devices. Statistics from 12 devices for each sample.

Table S1. PV device parameters of the PSCs with different concentrations of Indigo measured under the reverse scan.

Indigo (mg/mL)	V_{oc}（V）	J_{sc}（mA/cm^2）	FF	PCE (%)
0.000	1.07	24.15	0.78	20.18
0.025	1.10	24.73	0.79	21.44
0.050	1.12	25.00	0.80	22.40
0.100	1.10	24.30	0.78	20.85
0.250	1.10	23.70	0.79	20.54
0.500	1.09	23.73	0.79	20.43
1.000	1.08	23.34	0.77	19.41

Table S2. Fitting parameters of decay amplitude and decay time obtained from TRPL spectra.

	A_1	τ_1 (ns)	A_2	τ_2 (ns)	τ_{avg} (ns)
Pristine	586.55	2.99	108.94	315.27	300.01
Indigo (0.05 mg/mL)	475.24	4.51	111.59	473.24	454.94

Table S3. EIS parameters of devices based on pristine and Indigo-treated perovskite.

	R_{tr} (Ohm)	R_{rec} (Ohm)	C_{rec} (F)
Control	32.95	116.5	7.41×10^{-9}
Target	30.39	267.2	5.71×10^{-9}